Available online at www.sciencedirect.com
ScienceDirect
International Communications in Heat and Mass Transfer 34 (2007) 304–312
International Communications in HEAT and MASS TRANSFER
www.elsevier.com/locate/ichmt

Dimensional analysis for the heat transfer characteristics in the corrugated channels of plate heat exchangers ☆

J.H. Lin, C.Y. Huang, C.C. Su *

Department of Mechanical Engineering, National Taiwan University, No. 1, Sec. 4, Roosevelt Road, Taipei 10617, Taiwan, ROC

Available online 16 January 2007

Abstract

Using the Buckingham Pi theorem, this study derives dimensionless correlations to characterize the heat transfer performance of the corrugated channel in a plate heat exchanger. The experimental data are substituted into these correlations to identify the flow characteristics and channel geometry parameters with the most significant influence on the heat transfer performance. Simplified correlations by omitting the factors with less influence are then obtained. The results show that Nu_x is affected primarily by Re, R/D_h, x/D_h, and β. Neglecting the minor effect of factors on Nu_x, it is shown that Nu_m is determined primarily by Re, R/D_h and β.

Keywords: Corrugated channel; Buckingham Pi theorem; Dimensionless correlation; Nusselt number; Forced convection

1. Introduction

Plate heat exchangers (PHEs) are widely applied throughout industry and are commonly designed with a corrugated channel surface resulting in the enhanced heat transfer performance by increasing the area over which heat transfer takes place and generating a vigorous mixing effect within the working fluid.

In the literature [1,2], it is shown that the use of a corrugated channel results in a more complex flow structure and improves the heat transfer by as much as two or three times compared to a conventional straight channel. In [3–6], the authors demonstrated that sinusoidal wavy plate arrangements and channel geometries improved the heat transfer performance by increasing the surface area and prompting the formation of vortexes in the flow. The symmetric arrangement yields a superior heat transfer performance to an asymmetric arrangement. Unfortunately, the geometric parameters are not expressed clearly. For this reason, in [7,8], the authors conducted a systematic investigation into the relative effects of W, λ, β, and the ratio of the radius of curvature of the channel to the length of the straight section. The results revealed that Nu_x increased with Re, but decreased with the extension of the axial.

In [9,10], the flow field and heat transfer characteristics within fully developed region of corrugated channels were analyzed numerically and the predicted pressure drop within the corrugated channel was in good agreement with experimental observations. In [11,12], the authors compared the performance of asymmetric and symmetric channels

☆ Communicated by W.J. Minkowycz.

* Corresponding author.
E-mail address: chinchiasu@ntu.edu.tw (C.C. Su).

0735-1933/$ - see front matter © 2007 Published by Elsevier Ltd.
doi:10.1016/j.icheatmasstransfer.2006.12.002

Nomenclature

A	Cross-sectional area, m^2
A_s	Surface area, m^2
c_p	Specific heat at constant pressure, kJ kg^{-1} K^{-1}
D_h	Hydraulic diameter, m
f	Friction factor
H	Height of channel, m
h_x	Local heat transfer coefficient, kJ m^{-2} K^{-1}
j	Coburn factor
k	Thermal conductivity, kJ m^{-1} K^{-1}
$\dot{m}$	Mass flow rate, kg s^{-1}
Nu_m	Average Nusselt number
Nu_x	Local Nusselt number
P	Wetted perimeter, m
Pr	Prandtl Number
Q	Heat transfer rate, kW
R	Radius of curvature, m
Re	Reynolds number
T_b	Bulk temperature, K
T_m	Mean temperature, K
T_w	Wall temperature, K
V	Average velocity, m s^{-1}
W	Width of channel, m
x, y	Coordinates
λ	Wave length, m
β	Corrugated angle
ρ	Density of air, kg m^{-3}
μ	Viscosity of air, N s m^{-2}
$\Delta\theta_{fw}$	Temperature difference between flow and wall, K
ϕ	Coefficient of determination
ξ	Relative error

and showed that the influence of the asymmetric channel geometry on the flow resistance and heat transfer characteristics of the channel flow gradually diminished as the undulation and curvature of the channel surface were reduced. In [13], Wang and Chang identified that the flow field is characterized by laminar-flow and swirl-flow regimes with Reynolds Number and corrugated aspect ratio.

The studies presented above provide important insights into the correlation between the heat transfer and the geometry characteristics of the corrugated channel. However, the definitions of the channel geometry parameters are generally different in each study and the quantities of the investigated channels were not enough slightly. Accordingly, the present study performs experimental trials and applies the Buckingham Pi theorem to develop a set of dimensionless correlations relating Nu_x and Nu_m to the flow conditions and the geometry parameters of the corrugated channel. The experimental measurements of Nu_x and Nu_m are then compared with the results calculated from the correlations in order to analyze the relative errors of the correlations.

2. Experimentation

Fig. 1 presents the principal geometry parameters and illustrates the experimental setup established to investigate the heat transfer characteristics in the corrugated channel for different flow conditions. The basic components of the experimental apparatus include a water loop, an air loop, and a measurement system. The water loop comprises a water

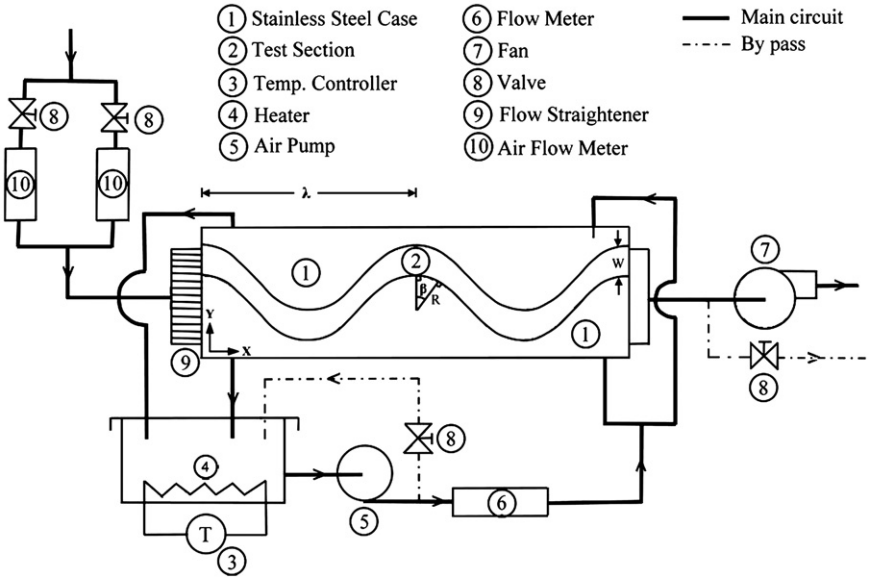

Fig. 1. Schematic illustration of experimental setup and geometry parameters.

tank containing a heater, a pump, a flow meter, and a temperature controller. Importantly, all of the components in the water system are thermally insulated such that the wall temperature of the corrugated channel can be maintained at a nearly constant temperature. The air loop consists of the test section containing the corrugated channel, a blower, two air flow meters, and a number of valves which enable the flow rate to be adjusted. Additionally, a flow straightener is installed at the entrance of the test section to maintain a uniform inlet flow. The test section is constructed from two hollow stainless steel 304 cases, each with a corrugated surface on one side and a flat surface on the other. The two cases are clipped between two horizontal, metal plates to form the corrugated channel through which the working fluid (air) is passed. During the experiments, hot water was flowed through the two hollow cases to maintain the channel surfaces at an approximately constant temperature and T-type thermocouples wrapped in copper tubes and inserted into upper metal plates were used to record the corresponding air temperature. The side effect was avoided by specifying a small aspect ratio for the channel such that variations in the channel height could be neglected. In the experiments, the temperature distribution in the horizontal, middle plane of the channel was monitored using thermocouples positioned at more than 200 different locations along the length of the channel. The precise number of measuring points was varied in accordance with the parameters W, R and β. For each test condition, two to three measurements were made in this study.

3. Dimensional analysis and data reduction

Using the Buckingham Pi theorem, a set of dimensionless correlations were established to investigate the heat transfer characteristics within the corrugated channel. The following procedure was adopted to determine the dimensionless parameters, π: (1) list the corresponding parameters; (2) apply the MLtθ system; (3) list the dimensions of all the parameters; and (4) let ρ, μ, D_h and k denote the repeating variables. The local heat transfer coefficient, h_x, is given by:

$$h_x = f(\rho, \mu, D_h, k, V, x, R, \beta, c_p, \Delta\theta) \tag{1}$$

where the hydraulic diameter is defined as:

$$D_h = \frac{4A}{P} = \frac{2WH}{W+H} \tag{2}$$

The dimensionless parameter groups Π_1–Π_7 listed in Table 1 are obtained through the procedures described above. The dimensionless correlation of the heat transfer performance within the channel can be expressed as:

$$\Pi_1 = a \cdot \Pi_2^b \cdot \Pi_3^c \cdot \Pi_4^d \cdot \Pi_5^e \cdot \Pi_6^f \cdot \Pi_7^g \tag{3}$$

where Π_1, Π_4, Π_6, and Π_7 are calculated from the measured temperature data within the fully developed region. Applying the differential control volume concept and the energy conservation law, it can be shown that:

$$\mathrm{d}Q = \cdot mc_\mathrm{p}[(T_\mathrm{m})_{x+\mathrm{d}x} - (T_\mathrm{m})_x] = h_\mathrm{x}(T_\mathrm{w} - T_\mathrm{b})\mathrm{d}A_\mathrm{s} \tag{4}$$

$$T_\mathrm{b} = \frac{(T_\mathrm{m})_x + (T_\mathrm{m})_{x+\mathrm{d}x}}{2} \tag{5}$$

and

$$T_\mathrm{m} \equiv \frac{\int \rho u c_\mathrm{p} T \mathrm{d}A}{\int \rho u c_\mathrm{p} \mathrm{d}A} \tag{6}$$

Combining Eqs. (4)–(6), the local heat transfer coefficient can be expressed as:

$$h_\mathrm{x} = \frac{\cdot \mathrm{m} c_p[(T_\mathrm{m})_{x+\mathrm{d}x} - (T_\mathrm{m})_x]}{(T_\mathrm{w} - T_\mathrm{b})\mathrm{d}A_s} \tag{7}$$

Therefore, it can be shown that:

$$Nu_\mathrm{x} \equiv \frac{h_\mathrm{x} D_\mathrm{h}}{k} = \frac{\cdot mc_\mathrm{p}[(T_\mathrm{m})_{x+\mathrm{d}x} - (T_\mathrm{m})_x]WH}{k(W+H)(T_\mathrm{w} - T_\mathrm{b})\mathrm{d}A_\mathrm{s}} \tag{8}$$

and

$$Nu_\mathrm{m} \equiv Nu_{a-b} = \frac{\int_a^b Nu_\mathrm{x} \mathrm{d}A_\mathrm{s}}{\int_a^b \mathrm{d}A_\mathrm{s}} \tag{9}$$

where a and b indicate different cross-sections of the channel.

In Eq. (10) presented in Table 2a, the value of constant a and the exponents b–g of the Π parameters are obtained by substituting the experimental data into Eq. (3) using STATISTICA statistical software. Subsequently, omitting each parameter in turn, Eqs. (11)–(16) can be obtained. Comparing Eq. (11) to Eq. (16), it is observed that the effects of Π_6 and Π_7 on Π_1 are minor. Accordingly, Eq. (17) is obtained by neglecting the effects of Π_6 and Π_7 in Eq. (10).

Fig. 2 compares the measured Nu_x with those predicted using Eq. (10). From inspection, ϕ is found to be 0.914 and the range of ξ varies from −30% to 30%. Here, ϕ is a relative comparison criterion between the measured and the

Table 1
Dimensionless $\prod$ groups

Groups	Definition	Effect	Range
Π_1	$h_\mathrm{x}D_\mathrm{h}/k$	Local Nusselt number	–
Π_2	$\rho V D_\mathrm{h}/\mu$	Reynolds number	300–7000
Π_3	R/D_h	Geometry	1.21–3.25
Π_4	x/D_h	Location	1–14.5
Π_5	β	Geometry	$\pi/12$–$\pi/4$
Π_6	$\rho^2 D_\mathrm{h}^2 k \Delta\theta/\mu^3$	Temperature difference	1.328E+11–10.507E+11
Π_7	$\mu c_\mathrm{p}/k$	Prandtl number	0.703–0.706
Π_8	$h_\mathrm{m}D_\mathrm{h}/k$	Average Nusselt number	–

Table 2a
Dimensionless correlation for Nu_x: $\prod_1 = a \cdot \prod_2^b \cdot \prod_3^c \cdot \prod_4^d \cdot \prod_5^e \cdot \prod_6^f \cdot \prod_7^g$

	a	b	c	d	e	f	g	Eq. number
Π_1	$10^{-2.79}$	0.912	0.334	−0.282	0.198	0.104	0.010	(10)
$\Pi_{1,a}$	$10^{-8.53}$	–	0.820	0.068	0.241	0.813	0.246	(11)
$\Pi_{1,b}$	$10^{-0.72}$	0.922	–	−0.337	0.174	−0.066	0.029	(12)
$\Pi_{1,c}$	$10^{-6.13}$	0.893	0.475	–	0.221	0.376	0.003	(13)
$\Pi_{1,d}$	$10^{-2.58}$	0.914	0.307	−0.292	–	0.083	0.015	(14)
$\Pi_{1,e}$	$10^{-1.54}$	0.919	0.251	−0.333	0.189	–	0.014	(15)
$\Pi_{1,f}$	$10^{-2.82}$	0.913	0.338	−0.282	0.200	0.106	–	(16)
$\Pi_{1,g}$	$10^{-1.52}$	0.921	0.255	−0.333	0.190	–	–	(17)

predicted data and ξ indicate the maximum deviation of the experimental data from the predicted values. As ϕ approaches a value of 1, the predicted data converge to the measured data. The mathematic definitions of ϕ and ξ are given respectively by:

$$\phi = \frac{\sum(\Pi_{1,\text{pred}} - \overline{\Pi}_{1,\text{meas}})^2}{\sum(\Pi_{1,\text{meas}} - \overline{\Pi}_{1,\text{meas}})^2} \tag{18}$$

$$\xi = \frac{(\Pi_{1,\text{meas}} - \Pi_{1,\text{pred}})}{\Pi_{1,\text{pred}}} \tag{19}$$

where $\Pi_{1,\text{meas}}$ is the measured data of Π_1, $\Pi_{1,\text{pred}}$ is the predicted data calculated from Eq. (3), and $\overline{\Pi}_{1,\text{meas}}$ is the average value of the measured data of Π_1.

4. Results and discussion

In the straight duct, the Nu_x converges to a constant value within the fully developed region. However, in the case of the corrugated channel, Fig. 3 indicates that the value of Nu_x reduces with increasing x/D_h. Furthermore, it is evident that Nu_x attains a local peak at the individual crests of the channel surface. This result is very different from that observed in a straight duct. Therefore, the heat transfer characteristics discussed below are related to the fully developed region, as defined by Lee et al. [7].

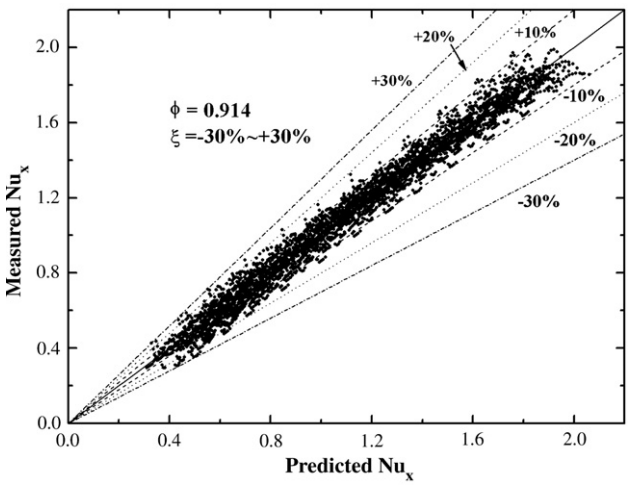

Fig. 2. Measured Nu_x versus Nu_x computed using Eq. (10).

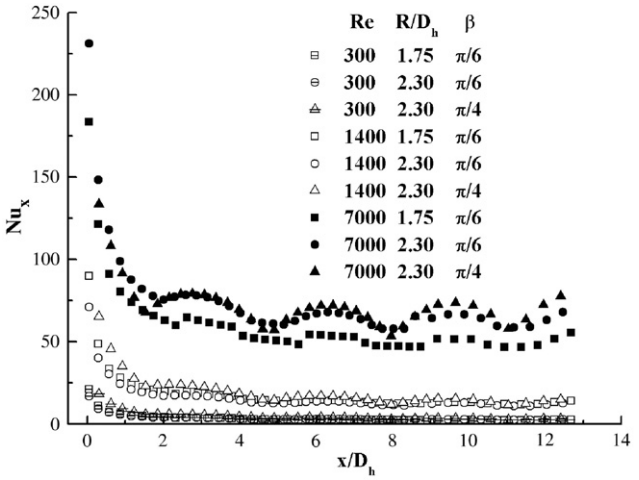

Fig. 3. Variation of Nu_x along channel length.

4.1. Nu_x and Nu_m

Observing the exponents in Eq. (10), it is seen that Nu_x increases with increasing Re, R/D_h, β, $\Delta\theta_{fw}$ and Pr_x, but decreases with increasing x/D_h. As shown in Table 1, Π_8 corresponds to Nu_m, and is computed with Eq. (9). Therefore, the effect of Π_4, Π_6, and Π_7 can be neglected in developing an expression for Π_8, i.e.

$$\Pi_8 = A \cdot \Pi_2^B \cdot \Pi_3^C \cdot \Pi_5^D \tag{20}$$

The experimental data obtained for Nu_m in the fully developed region are substituted into Eq. (20) using statistical software to yield Eq. (21), shown in Table 2b. From the exponents in Eq. (21), it can be seen that Nu_m increases with increasing Re, R/D_h and β. Fig. 4 compares the measured Nu_m with those predicted from Eq. (21). From inspection, ϕ is 0.985 and ξ varies between −20% and 30%. From the variations of the exponents in Eqs. (10) and (21), it can be inferred that Nu_x and Nu_m are affected by the factors listed in Table 1, respectively.

4.2. Effect of Reynolds number

With a value of 0.912, exponent b of Π_2 is the highest of all the exponents in Eq. (10). This not only indicates that Nu_x increases with increasing Re, but also implies that the effect of Re on Nu_x is more significant than that of any of the other factors. As shown in

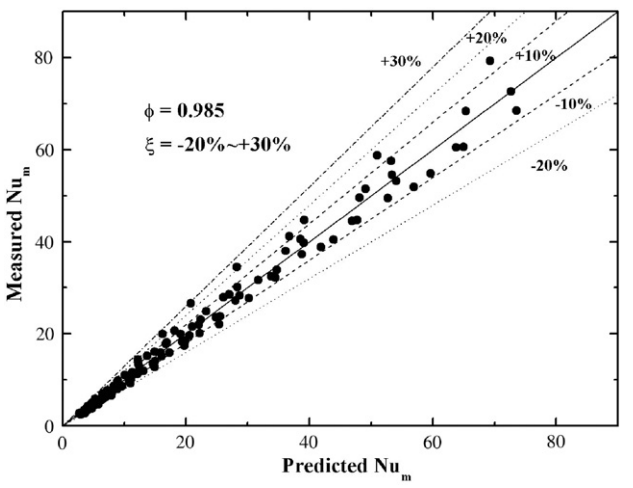

Fig. 4. Measured Nu_m versus Nu_m computed using Eq. (21).

Table 2b
Dimensionless correlation for Nu_m: $\prod_8 = A \cdot \prod_2^B \cdot \prod_3^C \cdot \prod_5^D$

	A	B	C	D	Eq. number
Π_8	$10^{-1.747}$	0.914	0.338	0.258	(21)

Fig. 3, at a low value of *Re*, the variation of Nu_x with increasing x/D_h is relatively minor with increasing R/D_h and β. For a given value of D_h, a higher *Re* prompts the formation of flow vortexes around the crests of the channel surface with increasing inlet velocity. These vortexes cause the flow to become turbulent, resulting in an enhanced mixing effect. Consequently, the value of Nu_x increases. Furthermore, at high *Re*, Nu_x increases notably with increasing R/D_h and β. The exponent *B* in Eq. (21) has a value of 0.914, which is in good agreement with the results of Fig. 5, which shows that Nu_m increases strongly with increasing *Re*. When *Re* is omitted in Eq. (11), ϕ reduces to 0.133. Hence, the dimensionless analysis confirms that *Re* has the most significant effect on Nu_x and Nu_m.

4.3. Effect of radius of curvature

In Eq. (10), the exponent *c* of Π_3 has a value of 0.334, which indicates that Nu_x increases with R/D_h. As shown in Figs. 3 and 5, for the case of $Re = 7000$ and $\beta = \pi/6$, the R/D_h increase from 1.75 to 2.30 implies that the ratio of the length of the straight section of the channel to the total length of the channel decreases. Therefore, by implication, the ratio of the length of the corrugated section of the channel to the total length of the channel increases. The flow in the straight section of the channel tends to become laminar. However, the fluid experiences a greater disturbance in the corrugated region of the channel with increasing R/D_h. The reduction in the wave amplitude of the corrugated section of the channel with increasing R/D_h weakens the vortexes generated around the corrugated section. Nevertheless, the overall result show that Nu_x still increases by approximately 20–40% and Nu_m increases by approximately 30%. These results are consistent with the numerical results presented by Yang and Chang [14]. As shown in Eqs. (10) and (21), the effect of R/D_h on the Nusselt number is greater than that of β. An increased value of β induces vortexes within the channel as a result of the flow separation. The enhanced mixing effect enhances the heat transfer rate on the one hand, but reduces the effective heat transfer area resulting in a reduction in the heat transfer rate on the other. The overall result is that the effect of R/D_h on the heat transfer performance is greater than that of β. The exponent *C* in Eq. (21) has a value of 0.338, which confirms that Nu_m increases with increasing R/D_h and has a greater effect on Nu_m than β. When R/D_h is omitted, ϕ reduces from 0.914 to 0.875 and ξ varies between −38% and 38%. Fig. 6 compares the predicted Nu_m using Eq. (21) with those calculated by Lee [15]. From inspection, ξ varies between −20% and 40%.

4.4. Effect of distance from entrance

Exponent *d* of Π_4 in Eq. (10) has a value of −0.282, which implies that Nu_x decreases with increasing x/D_h. As shown in Fig. 3, as the thermal boundary layer of the fluid in the entrance region grows, the temperature gradient of the fluid near the wall decreases with increasing x/D_h. Therefore, Nu_x reduces with reducing h_x as x/D_h increases. In a straight duct, for a given value of *Re*, Nu_x converges to a

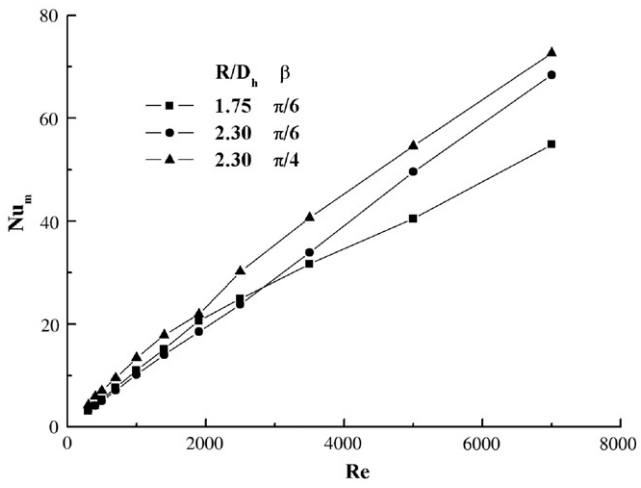

Fig. 5. Relationship between Nu_m and *Re*.

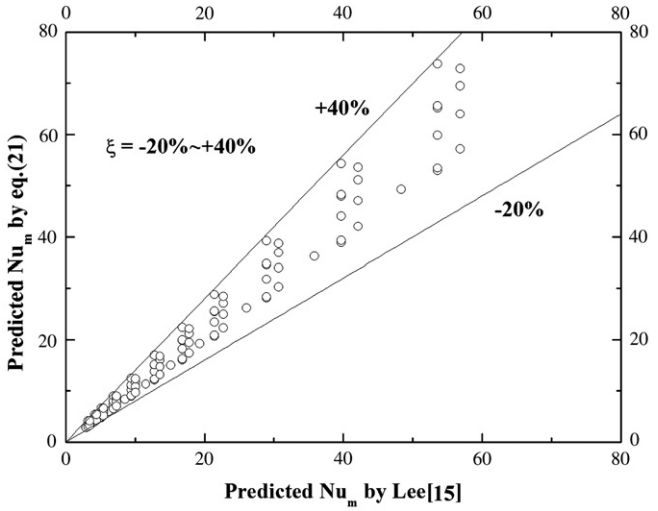

Fig. 6. Nu_m computed using Eq. (21) versus Nu_m predicted by Lee [15].

constant value in the fully developed region, and hence the effect of x/D_h need not be considered. However, in the present corrugated channel, the vortexes generated near the crests of the channel cause a local increase in Nu_x. Note that these results are consistent with the numerical findings presented by Rush et al. [5]. In other words, x/D_h has an important influence on Nu_x in the corrugated channel. When the effect of x/D_h is neglected in Eq. (13), ϕ reduces from 0.914 to 0.889 and the range of ξ varies from −35% to 38%.

4.5. Effect of corrugated angle

Exponent e of Π_5 in Eq. (10) has a value of 0.198, while exponent D of Π_6 in Eq. (21) has a value of 0.258. These results indicate that both Nu_x and Nu_m increase with increasing β. The abrupt change induced in the direction of flow of the fluid as β increases enhances the heat transfer rate. As shown in Fig. 3, for given values of Re, R/D_h and x/D_h, Nu_x increases with increasing β. Similarly, in the case of $Re=3500$ and $R/D_h=2.30$ shown in Fig. 5, Nu_m increases by approximately 25% as β increases from $\pi/6$ to $\pi/4$. The increased value of β causes the laminar flow within the channel to transit to turbulent flow at a lower value of Re. For example, for a constant value of $R/D_h=2.30$, Nu_m in the case of $\beta=\pi/4$ and $Re=1900$ is roughly the same as that in the case of $\beta=\pi/6$ and $Re=2500$. Therefore, omitting factor β in Eq. (14) causes ϕ to reduce from 0.914 to 0.895 and ξ to vary between −32% and 35%. Hence, it is apparent that the corrugated angle of the channel has a significant effect on the value of the Nusselt number.

4.6. Effect of local temperature difference and local Prandtl number

Exponent f of Π_6 in Eq. (10) has a value of 0.104, and hence it can be inferred that $\Delta\theta_{fw}$ of the flow entering the fully developed region converges gradually to a constant. This implies that the increases in Nu_x in the regions around the crests of the channel are caused primarily by variations in R/D_h and β rather than by that in $\Delta\theta_{fw}$. When $\Delta\theta_{fw}$ is omitted in Eq. (15), ϕ decreases from 0.914 to 0.910 and ξ varies from −35% to 33%. Exponent g of Π_7 in Eq. (10) has a value of 0.010 and is the lowest of any of the exponents. Therefore, it can be surmised that the effect of Pr_x on Nu_x is less than that of any of the other factors. This result is reasonable since this study uses air as the working fluid. The variation of μ, c_p and k for air in the measured range is less than one percent, and therefore the effect of Pr_x on Nu_x and Nu_m, respectively, investigated in Eq. (21) can be neglected. When Pr_x is omitted in Eq. (16), ϕ decreases slightly from 0.914 to 0.911 and the range of ξ varies between −35% and 30%.

5. Conclusions

This study has developed dimensionless correlations for analyzing the heat transfer characteristics of the corrugated channel used in a PHE. The major contributions and analytical findings of this study can be summarized as follows:

1. Dimensionless correlations for Nu_x and Nu_m have been developed based on experimental results and the Buckingham Pi theorem. Compared with the experimental results, the accuracies of the dimensionless correlations are found to be acceptable.

2. The dimensionless analysis reveals that Nu_x is determined primarily by Re, R/D_h, x/D_h and β. Conversely, Pr_x and $\Delta\theta_{fw}$ do not have a significant effect on the heat transfer performance.
3. The value of the mean Nusselt number, Nu_m, is determined principally by Re, R/D_h and β.

Acknowledgement

The current authors gratefully acknowledge the financial support provided to this study by the National Science Council of Taiwan under Contract No.SC90-2212-E-002 -201.

References

[1] J.E. O'Brien, E.M. Sparrow, Corrugated-duct heat transfer, pressure drop and flow visualization, Trans. ASME, J. Heat Transfer 104 (1982) 410–416.
[2] L. Goldstein Jr., E.M. Sparrow, Heat/mass transfer characteristics for flow in a corrugated wall channel, Trans. ASME, J. Heat Transfer 99 (1977) 187–195.
[3] T. Nishimura, S. Murakami, S. Arakawa, Y. Kawamura, Flow observations and mass transfer characteristics in symmetrical wavy-walled channels at moderate Reynolds numbers for steady flow, Int. J. Heat Mass Transfer 33 (1990) 835–845.
[4] T. Nishimura, K. Yano, T. Yoshino, Y. Kawamura, Occurrence and structure of Taylor–Goertler vortices induced in two-dimensional wavy channels for steady flow, J. Chem. Eng. Jpn. 23 (1990) 697–703.
[5] T.A. Rush, T.A. Newell, A.M. Jacobi, An experimental study of flow and heat transfer in sinusoidal wavy passages, Int. J. Heat Mass Transfer 42 (1999) 1545–1553.
[6] A. Muley, R.M. Manglik, Experimental study of turbulent flow heat transfer and pressure drop in a plate heat exchanger with chevron plates, Trans. ASME, J. Heat Transfer 121 (1999) 110–117.
[7] Y.S. Lee, Y.M. Sun, C.C. Su, Experimental study of heat transfer of corrugated channels, 1st International Conference on Heat, Fluid Mechanics, and Thermodynamics, 2002, pp. 505–510.
[8] Y.S. Lee, C.C. Su, Y.M. Sun, J.C. Ye, Experimental study on heat transfer in wavy channels, J. Enhanc. Heat Transf. 10 (2003) 21–29.
[9] L.C. Yang, Y. Asako, Y. Yamaguchi, M. Faghri, Numerical prediction of transitional characteristics of flow and heat transfer in a corrugated duct, Trans. ASME, J. Heart Transfer 119 (1997) 62–69.
[10] Y. Asako, M. Faghri, Finite-volume solutions for laminar flow and heat transfer in a corrugated duct, Trans. ASME, J. Heat Transfer 109 (1987) 627–634.
[11] Q. Xiao, R.C. Xin, W.Q. Tao, Analysis of fully developed laminar flow and heat transfer in asymmetric wavy channels, Int. Commun. Heat Mass Transf. 16 (1989) 227–236.
[12] R.C. Xin, W.Q. Tao, Numerical prediction of laminar flow and heat transfer in wavy channels of uniform cross-sectional area, Numer. Heat Transf. 14 (1989) 465–481.
[13] C.C. Wang, C.K. Chang, Forced convection in a wavy-wall channel, Int. J. Heat Mass Transfer 45 (2002) 2587–2595.
[14] R. Yang, S.F. Chang, A numerical study of fully developed laminar flow and heat transfer in a curved pipe with arbitrary curvature ratio, Int. J. Heat Fluid Flow 14 (1993) 138–145.
[15] Y.S. Lee, Experimental studies of small vapor-compression refrigeration system & wavy channels with plate heat exchanger, PhD Dissertation, Dept. of Mech. Eng., National Taiwan University, Taiwan (2003) 81.